# Cell-type-specific fluorescent tagging of endogenous target proteins reveals synaptic enrichment and dynamic regulations of dopamine receptors

Shun Hiramatsu[1], Kokoro Saito[1], Shu Kondo[2], Hidetaka Katow[3], Nobuhiro Yamagata[4], Chun-Fang Wu[5], Hiromu Tanimoto[1]

[1] Graduate School of Life Sciences, Tohoku University.
[2] Department of Biological Science and Technology, Faculty of Advanced Engineering, Tokyo University of Science.
[3] Department of Cell Biology, New York University.
[4] Faculty and Graduate School of Engineering Science, Akita University.
[5] Department of Biology, University of Iowa.

## Abstract

Dopamine can play opposing physiological roles depending on the receptor subtype. In the fruit fly *Drosophila melanogaster*, *Dop1R1* and *Dop2R* encode the $D_1$- and $D_2$-like receptors, respectively, and are reported to oppositely regulate intracellular cAMP levels. Here, we profiled the expression and subcellular localization of endogenous Dop1R1 and Dop2R in specific cell types in the mushroom body circuit. For cell-type-specific visualization of endogenous proteins, we employed reconstitution of split-GFP tagged to the receptor proteins. We detected dopamine receptors at both presynaptic and postsynaptic sites in multiple cell types. Quantitative analysis revealed enrichment around the active zones, particularly for Dop2R. The presynaptic localization of Dop1R1 and Dop2R in dopamine neurons suggests dual feedback regulation as autoreceptors. Furthermore, we discovered a starvation-dependent, bidirectional modulation of the presynaptic receptor expression in the PAM and PPL1 clusters, two distinct subsets of dopamine neurons, suggesting regulation of appetitive behaviors. Our results highlight the significance of the co-expression of the two antagonizing dopamine receptors in the spatial and conditional regulation of dopamine responses in neurons.

## Introduction

Neurotransmitters typically have multiple cognate receptors, and they may recruit different second messenger systems. Therefore, the expression and localization of receptor subtypes are critical for determining cellular responses to neurotransmitter inputs. The dopaminergic system offers an ideal *in-vivo* study case to this end, as it regulates a wide array of physiological functions through combinations of different receptor subtypes. In mammals, $D_1$-like receptors are coupled to $G\alpha_s$, thereby activating adenylate cyclase upon ligand binding, whereas $G\alpha_i$-coupled $D_2$-like receptors inhibit cyclase activity (Beaulieu & Gainetdinov, 2011). Four dopamine receptors have been identified in *Drosophila*: *Dop1R1*, *Dop1R2*, *Dop2R*, and *DopEcR* (K. A. Han et al., 1996; Hearn et al., 2002; Srivastava et al., 2005; Sugamori et al., 1995). *Dop1R1* and *Dop2R* correspond to the $D_1$- and $D_2$-like receptors, respectively (Hearn et al., 2002; Sugamori et al., 1995). *Dop1R2* and *DopEcR* are invertebrate-specific and have been reported to recruit different second messenger systems (K. A. Han et al., 1996; Srivastava et al., 2005). Intriguingly, recent data of single-cell RNA-seq and transgenic expression profiling revealed that the expression of these dopamine receptors is highly overlapping in the fly brain (Croset et al., 2018; Davie et al., 2018; Dolan et al., 2019; Kondo et al., 2020), unlike the spatially segregated expression of the $D_1$- and $D_2$-like receptors in vertebrate brains (Gerfen & Surmeier, 2011). Considering the opposing physiological roles of the *Dop1R1* and *Dop2R*, their protein localization especially in those cells where they are coexpressed should be critical to determine the responses to the dopamine inputs.

*Drosophila* mushroom bodies (MB) have long served as a unique dopaminergic circuit model to study adaptive behaviors, such as associative memory. MB-projecting neurons and their connections have been systematically described at both mesoscopic and ultrastructural resolutions (Aso, Hattori, et al., 2014; Li et al., 2020; Takemura et al., 2017; Tanaka et al., 2008). Kenyon Cells (KCs), the major MB intrinsic neurons, encode a variety of sensory information (Honegger et al., 2011; Turner et al., 2008; Vogt et al., 2014). Intriguingly, each KC receives synaptic inputs from different dopaminergic projections in multiple spatially segmented compartments along its axon in the MB lobe (Aso, Hattori, et al., 2014; Tanaka et al., 2008). MB-projecting dopamine neurons (DANs) originate from the three cell clusters (Mao & Davis, 2009; Nässel & Elekes, 1992). DANs in the protocerebral posterior lateral 1 (PPL1) cluster project to the vertical lobes and the peduncle of the MB, and they control different aspects of associative memory (Aso et al., 2010, 2012; Aso & Rubin, 2016; Claridge-Chang et al., 2009; Krashes et al., 2009; Mao & Davis, 2009; Masek et al., 2015; Riemensperger et al., 2005; Takemura et al., 2017; Vogt et al., 2014). The protocerebral anterior medial (PAM) cluster, the largest DAN cluster, mostly projects to the medial lobes of the MB, and many PAM neurons are involved in reward processing (Burke et al.,

2012; Felsenberg et al., 2018; Huetteroth et al., 2015; Ichinose et al., 2021; Lin et al., 2014; Liu et al., 2012; Yamagata et al., 2015, 2016). DANs in PPL2ab project to the MB calyx and control the conditioned odor response (Boto et al., 2019). In addition to the variety of the dopamine sources, KCs express all four dopamine receptor subtypes (Deng et al., 2019; Kondo et al., 2020). Given the multitude of modulatory effects of dopamine in the MB (Berry et al., 2018; Cohn et al., 2015; Handler et al., 2019), receptor localization in KCs provides important information for interpreting such functional diversity.

The projections and synapses of the neurons in the MB circuit are tightly intertwined (Li et al., 2020; Takemura et al., 2017). Therefore, conventional immunohistochemical approaches using light microscopy do not allow identification of cells from which immunoreactive signals originate. Precise determination of their subcellular localization requires visualization of the proteins of interest only in the target MB neurons (Fendl et al., 2020). Employing the CRISPR/Cas9-mediated split-GFP tagging strategy (D. Kamiyama et al., 2016; R. Kamiyama et al., 2021; Kondo et al., 2020), we profiled the spatial distribution of endogenous Dop1R1 and Dop2R proteins in KCs, the PAM, and the PPL1 DANs.

## Results

### Co-expression of *Dop1R1* and *Dop2R* genes in the adult *Drosophila* brain

To compare the expression of different dopamine receptor genes in detail, we used fluorescent reporter knock-ins of the endogenous *Dop1R1* and *Dop2R* genes (Kondo et al., 2020). Both lines labelled many neuropils including the MB (Figure 1A and 1B), and the overlapping expression of these receptors is consistent with our previous quantification of GAL4-positive cells for both genes (58,049 and 68,528 for *Dop1R1* and *Dop2R*, respectively, out of 118,331 brain cells; Kondo et al., 2020). Double labelling of *Dop1R1* and *Dop2R* with *T2A-LexA* and *T2A-GAL4*, respectively, revealed cells with overlapping and differential expression (Fig. 1D-G; see also Kondo et al., 2020). The PAM cluster of DANs expressed both *Dop1R1* and *Dop2R* (Figure 1D). On the other hand, most of the DANs in the PPL1 cluster strongly expressed *Dop2R*, but *Dop1R1* only weakly (Figure 1E). We further found that *Dop1R1*, but not *Dop2R*, was highly expressed in the ring neurons of the ellipsoid body (Figure 1F; Hanesch et al., 1989) and the neuropil ensheathing glia (Figure 1G; Awasaki et al., 2008). In conclusion, *Dop1R1* and *Dop2R* genes are co-expressed in

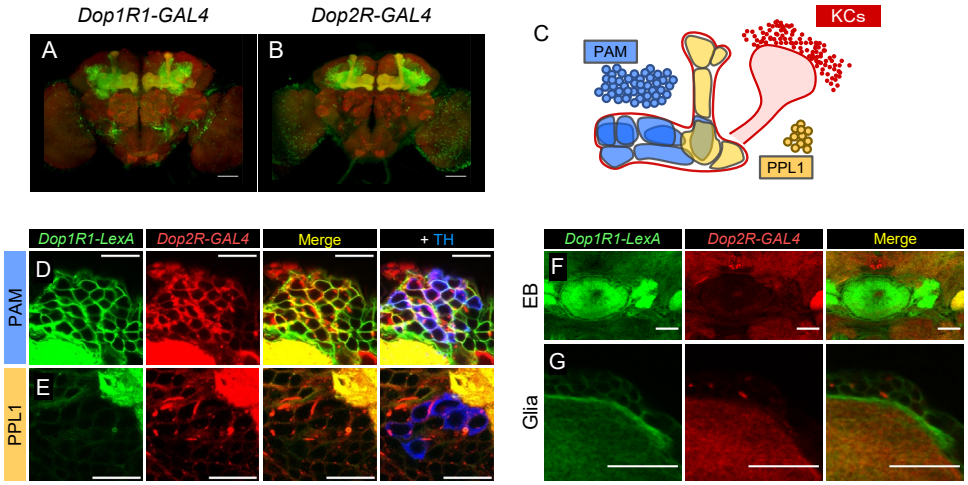


**Figure 1. Co-expression of *Dop1R1* and *Dop2R* genes in adult *Drosophila* brain.**

(A and B) The expression of *Dop1R1-T2A-GAL4* and *Dop2R-T2A-GAL4* visualized by *UAS-mCD8::GFP* (green) The neuropil was stained by using *Brp::SNAP* (red). Maximum-intensity projections of the whole brain.
(C) Schematic of the KCs and the MB-innervating dopamine neurons from the PAM and PPL1 clusters.
(D-G) Double labelling of *Dop1R1* and *Dop2R* gene expression visualized by *Dop1R1-T2A-LexA/lexAop-rCD2::GFP* (green) and *Dop2R-T2A-GAL4/UAS-CD4::tdTomato* (red). Dopamine neurons were immunostained with anti-TH antibody (blue). Single optical sections. Cell bodies of the PAM cluster (D) and the PPL1 cluster (E). The ellipsoid body (F) and ensheathing glia (G).
Scale bars, 50 µm (A and B), 5 µm (D-G).

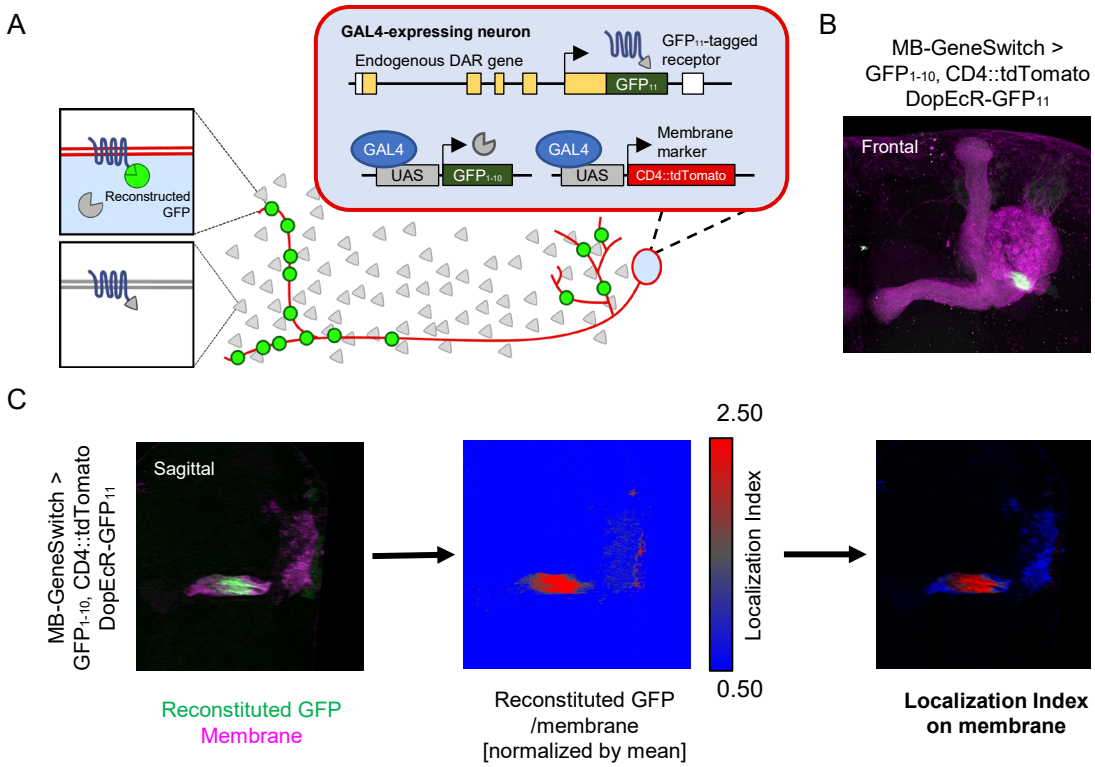


**Figure 2. Cell type-specific visualization of endogenous proteins with $GFP_{11}$ tag.**

(A) Principle of cell type specific fluorescent labelling of target proteins by $GFP_{11}$ tag. $GFP_{1-10}$ and membrane marker CD4::tdTomato are expressed in the target cells by GAL4/UAS system. In the target cells, reconstitution of GFP occurs on the endogenous proteins tagged with $GFP_{11}$.
(B) As an example, DopEcR::$GFP_{11}$ is visualized in KCs using *MB-GeneSwitch*, a ligand-inducible GAL4 driver. A merged image of reconstituted GFP (green) and cellular membrane visualized by *UAS-CD4::tdTomato* (magenta). Maximum intensity projection of the whole left MB.
(C) The workflow for visualizing subcellular protein enrichment by localization index (LI). A single sagittal section of the MB calyx and peduncle is shown. The ratio of reconstituted GFP to membrane signal in the left image is calculated and normalized by the mean intensity of all voxels to provide LI. In the middle image, LI is color-coded so that red represents local receptor enrichment. In the right image, the LI color is mapped on the membrane signal.

the PAM neurons, KCs and a subset of the PPL1 neurons.

## Quantification of subcellular enrichment of endogenous proteins in target cells

The overlapping expression of *Dop1R1* and *Dop2R* genes prompted us to examine the subcellular localization of these receptor proteins. To elucidate the localization of these broadly expressed receptors (Figure 1), we took advantage of split-GFP tagging of endogenous proteins (D. Kamiyama et al., 2016; Kondo et al., 2020). By adding $GFP_{11}$ tags to the C-termini of the Dop1R1 and Dop2R proteins, their intracellular distribution can be visualized specifically in cells expressing $GFP_{1-10}$ through split-GFP reconstitution (Figure 2A).

98

99 To quantify the subcellular enrichment of the receptors, we devised Localization Index
100 (LI). Briefly, LI is the normalized ratio of the reconstituted GFP (rGFP) signal to the reference
101 membrane marker signal (CD4::tdTomato). If the target and reference proteins had the identical
102 distribution, LI would be 1 everywhere. More or less concentrations of rGFP result in the LI larger
103 or smaller than 1, respectively (Figure 2; see also Methods for detail). LI was visualized as the
104 color of the membrane signals (Figure 2C). As proof of principle, mapping the LI of DopEcR-
105 rGFP signals in KCs highlighted enrichment in the proximal peduncle (Figure 2B, C), which
106 is consistent with the previous report (Kondo et al., 2020). This representation thus visualizes the
107 subcellular enrichment of the targeted receptors in the plasma membrane of GAL4-expressing
108 cells.

109 **Partial colocalization of Dop1R1 and Dop2R proteins**

110 First, we compared the localization of Dop1R1 and Dop2R proteins in KCs, where both receptor
111 genes were highly expressed (Figure 1D). Both receptors were distributed throughout KC
112 membranes with predominant enrichment in the MB lobes (Figure 3B-E). This lobe enrichment
113 was more pronounced for Dop2R than Dop1R1 (Figure 3F and 3G). LI measurements indicated
114 that Dop2R was approximately twice as enriched in the lobe as the average density across the
115 whole neuron, while the lobe enrichment of Dop1R1 was about 1.5 times the average (Figure 3H).
116 As KCs have major presynaptic sites in the MB lobes, we examined receptor localization
117 to the active zones (AZ) using antibodies against Brp, an AZ scaffolding protein (Wagh et al.,
118 2006). Interestingly, Dop1R1 and Dop2R proteins in KCs were tightly associated with the Brp
119 puncta in the lobe (Figure 4A and 4B). The distribution of Dop2R, compared to Dop1R1, showed
120 a greater association, as measured by the overlap of rGFP and Brp signals (Figure 4C). This was
121 consistent with the higher lobe enrichment of Dop2R (Figure 3H). The AZ localization
122 (Christiansen et al., 2011) of Dop1R1 and Dop2R was similar in the calyx (Figure 4 – figure
123 supplement 1), although the identity of presynaptic neurons is less clear.
124 To better resolve the presynaptic localization of DopR1 and Dop2R, we turned to "giant"
125 *Drosophila* neurons differentiated from cytokinesis-arrested neuroblasts in culture (Wu et al.,
126 1990). These "giant" neurons exhibit action potential firing patterns and neurotransmission
127 similar to those described in mature neurons (Saito & Wu, 1991; Yao and Wu, 2001; Yao et al.,
128 2000). Due to the large size of the cells, this system has advantages for investigating the
129 microanatomy of neurons (Saito & Wu, 1991; Wu et al., 1990; Yao et al., 2000). In the giant
130 neurons from the *Brp::SNAP* embryos (Kohl et al., 2014), we found punctate aggregation of Brp

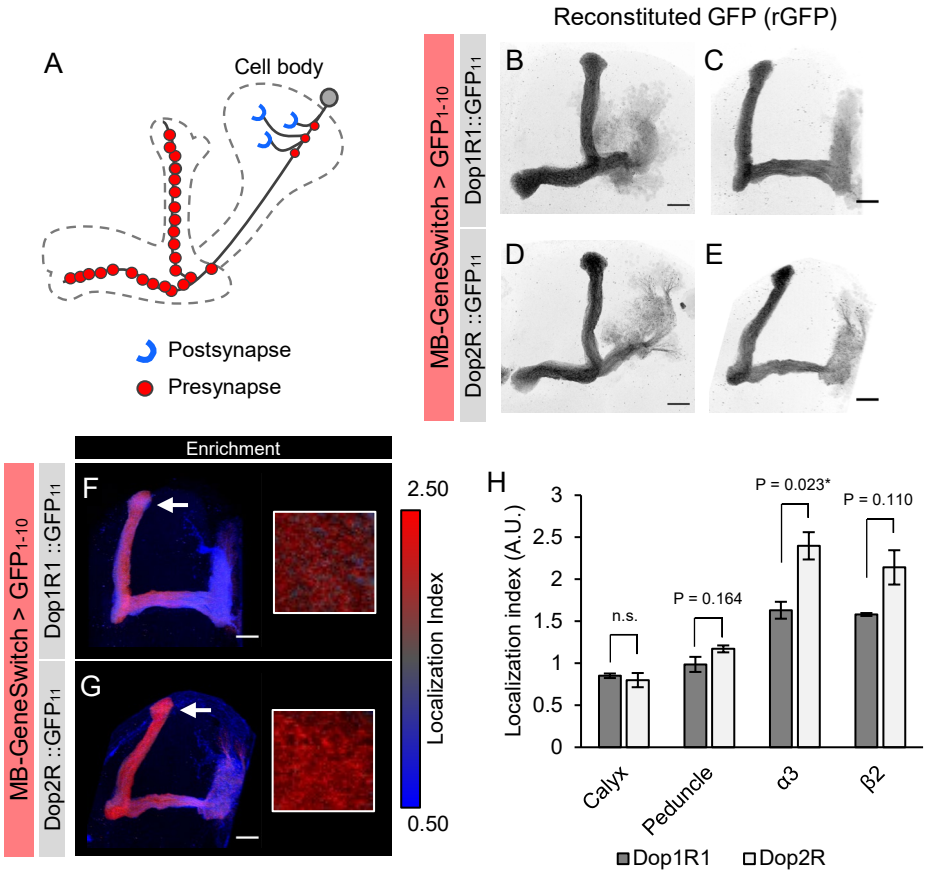


**Figure 3. Subcellular localization of Dop1R1 and Dop2R in the Kenyon Cells.**

Subcellular localization of Dop1R1 and Dop2R in the KCs is visualized by $GFP_{11}$-tag. *MB-GeneSwitch* was used to express $GFP_{1-10}$ and CD4::tdTomato in the KCs. Receptors in αβ KCs were visualized after 12 hours of RU486 feeding (see Materials and Methods).
(A) Schematic of the distribution of presynapses and postsynaposes in the KCs.
(B-G) Enrichment of Dop1R1 and Dop2R in the MB lobe. Frontal views of the MB (B and D) and sagittal views of the MB (C, E, F and G) of the maximum-intensity projections of the whole left MB are shown. Reconstituted GFP signals for both Dop1R1:: and Dop2R::$GFP_{11}$ distributed throughout the MB lobe and the calyx (B-E). Visualization by LI showed more pronounced enrichment of Dop2R (G) than Dop1R1 (F) in the lobe as exemplified in the tip (arrows, 10 µm square, magnified in the insertion). Scalebars, 20 µm (B-G).
(H) Mean LI for Dop1R1 and Dop2R in the calyx, the peduncle, the tip of α and β lobes. Student's t test was performed to compare LI of Dop1R1 and Dop2R in each region (N = 3). Error bars; SEM. * $p < 0.05$.

131 in the terminals of neurites, indicating the proper assembly of the AZ cytomatrix (Figure 4D and
132 4E). We confirmed that the giant neurons express Venus-tagged Dop1R1 and Dop2R (Figure 4F-
133 4I). Strikingly, double labelling of these receptors with Brp::SNAP showed the association, but
134 not overlap, with the Brp puncta, suggesting perisynaptic receptor accumulation (Figure 4F-4I).
135 A closer investigation revealed a tighter association between Dop2R and Brp (Figure 4G and 4I).
136 Presynaptic enrichment of these receptors in the giant neurons was strikingly similar to their

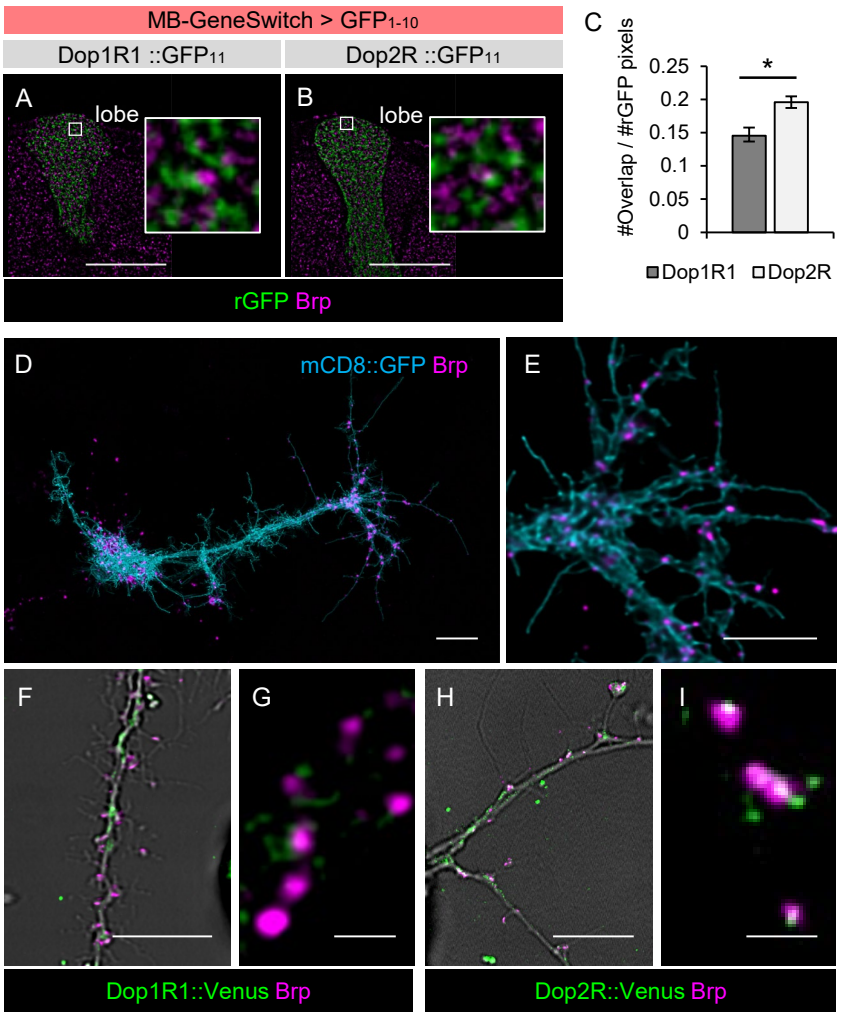


**Figure 4. Presynaptic localization of Dop1R1 and Dop2R in Kenyon Cells and giant neurons.**

(A and B) Double labelling of dopamine receptors (green) and Brp (magenta). Single focal slice at the tip of the vertical lobe. Insertions are the magnified images of white squares in the main panel.
(C) Colocalization analysis showed that Dop2R had significantly higher colocalization with Brp than Dop1R1 ($p = 0.0259$, Mann-Whitney U test, $N = 6$). Error bars; SEM.
(D-E) Punctate Brp expression in a giant neuron culture differentiated from cytokinesis-arrested neuroblasts of *OK371-GAL4/UAS-mCD8::GFP* embryos. Aggregated Brp condensates (magenta) were observed in the neurite terminals of the cells marked with mCD8::GFP (cyan) in (E).
(F-I) Double labelling of dopamine receptors (green) and the AZs (magenta). *Dop1R1::Venus* (F and G) or *Dop2R::Venus* (H and I) was crossed with *Brp::SNAP*.
Scale bars, 20 µm (A and B), 10 µm (D, F and H), 5 µm (E), 1 µm (G and I).

localization in KCs, further substantiating presynaptic dopaminergic modulation.

$D_2$-like receptors in mammals are expressed in DANs and act as autoreceptors, which mediates feedback signals by receiving neurotransmitters released from the neuron on which the receptors reside (Ford, 2014). In *Drosophila*, multiple dopamine receptor genes are expressed in

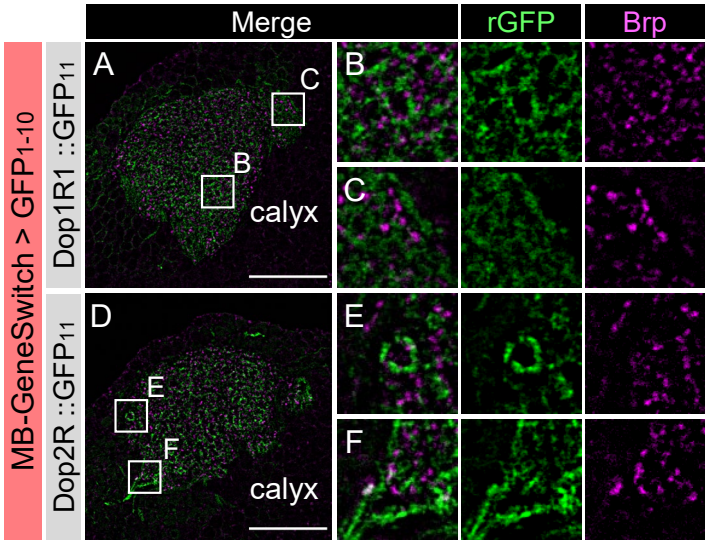


**Figure 4 – figure supplement 1. Dop2R and Dop1R1 at the presynaptic sites of Kenyon Cells in the calyx.**

(A-F) Double labelling of dopamine receptors (green) and Brp (magenta). From the single focal slice of the calyx (A and D), white squares including dendritic claws (B and E) and proximal dendrites (E and F) are magnified.
Scalebars, 20 µm (A and D).

141 DANs (Figure 1; Deng et al., 2019; Aso et al., 2019; Kondo et al., 2020), but it is unclear if these
142 receptors function as autoreceptors. We therefore examined the subcellular localization of
143 Dop1R1 and Dop2R in the PAM cluster DANs with a particular focus on their presynaptic
144 terminals. The PAM neurons are polarized; presynaptic proteins are abundantly enriched in the
145 MB lobe and barely detected in dendrites (Figure 5A-5C). We visualized Dop1R1 and Dop2R
146 proteins in the PAM cluster DANs using *R58E02-GAL4*, and both were localized to the terminals
147 in the MB lobes (Figure 5A and 5B). Representation of LI for Dop1R1 and Dop2R in the PAM
148 neurons again showed stronger presynaptic enrichment of Dop2R than Dop1R1 (Figure 5F and
149 5G). Dop2R was strongly enriched at β'1 compartment showing significantly higher LI than
150 Dop1R1 (Figure 5H-5J). Higher magnification revealed the accumulation of both Dop1R1 and
151 Dop2R in the boutons (Figure 5K and 5L). The presynaptic localization of Dop1R1 and Dop2R
152 in DANs suggests that both receptors mediate feedback regulation.

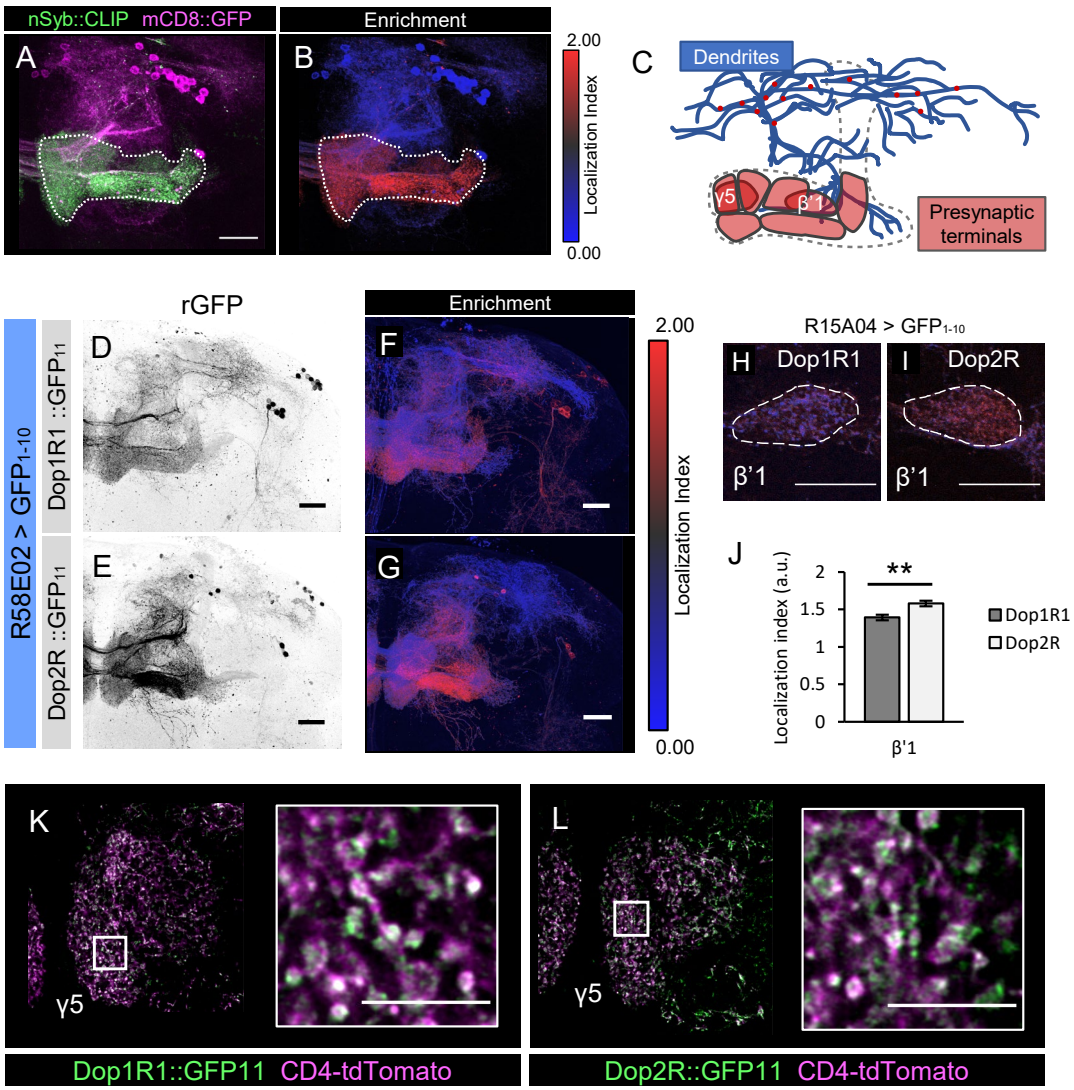


**Figure 5. Subcellular localization of Dop1R1 and Dop2R in dopamine neurons.**

(A-B) Maximum-intensity projection image showing the distribution of presynaptic sites in the PAM neurons. (A) *R58E02-GAL4* was used to express *UAS-mCD8::GFP* (magenta) and *UAS-nSyb-CLIP* (magenta). (B) Visualization by LI showing enrichment of nSyb signals in the lobe projection of the PAM neurons.
(C) Illustrated projection pattern of the PAM neurons. Red puncta indicate the sparse distribution of presynaptic sites in dendrites.
(D-L) Subcellular localization of $GFP_{11}$-tagged Dop1R1 and Dop2R in the PAM neurons. *R58E02-GAL4* was used to express *UAS-GFP$_{1-10}$* and *UAS-CD4::tdTomato* in the PAM neurons.
(D and E) Reconstituted GFP signals of Dop1R1::$GFP_{11}$ (D) and Dop2R::$GFP_{11}$ (E) in the PAM neurons. Maximum-intensity projections of the left hemisphere including the MB lobe, SMP, SIP and SLP (superior medial, intermediate, and lateral protocerebrum, respectively).
(F and G) Stronger presynaptic enrichment of Dop2R (G) than that of Dop1R1 (F) in the PAM dopamine neurons visualized by LI. β'1 compartment is magnified in the insertion image.

(H-J) *R15A04-GAL4* was used to measure LI in the PAM-β'1 neuron. (H and I) Presynaptic terminals of the PAM-β'1 neurons are shown (dashed line). (H) Mean LI for Dop1R1 and Dop2R in β'1 ($p = 0.0056$, Mann-Whitney U test, $N = 9$). Error bars; SEM.
(K and L) A single optical slice of γ5 compartment in the MB lobe obtained using Airyscan. Merged image of reconstituted GFP (green) and CD4::tdTomato (magenta). Insertions are the magnified images of the presynaptic boutons of PAM-γ5 (white squares).
Scale bars, 20 μm (A-B, D-I), 5 μm (K and L).

154 **State-dependent and bidirectional modulation of dopamine receptor expression in the PAM**
155 **and PPL1 DANs**

156 The activity of MB-projecting DANs is reported to be dynamic and sensitive to feeding states
157 (Ichinose et al., 2017; Liu et al., 2012; Plaçais & Preat, 2013; Senapati et al., 2019; Siju et al.,
158 2020; Tsao et al., 2018; Yamagata et al., 2016). We therefore examined if starvation alters the
159 protein expression of Dop1R1 and Dop2R in these MB-projecting DANs (Figure 6). We found a
160 significant elevation of Dop1R1 in the terminals of PAM-γ5 upon starvation for 10 hours or longer
161 (Figure 6E). In contrast, starvation did not increase Dop2R in PAM-γ5 but rather tended to
162 decrease, if at all (Figure 6E). We found similar starvation-dependent changes in Dop1R1 and
163 Dop2R levels in other PAM neurons (Figure6 – figure supplement 1A-H). These results together
164 suggest that starvation enhances presynaptic dopamine signaling in the reward-related PAM
165 neurons by shifting the balance of Dop1R1 and Dop2R.

166 DANs of the PAM and PPL1 clusters exert distinct, largely opposite behavioral functions
167 (Claridge-Chang et al., 2009; Liu et al., 2012). Therefore, plasticity in the PPL1 neurons may
168 differ from that in the PAM neurons. To test this hypothesis, we examined the starvation-
169 dependent change in Dop1R1 and Dop2R protein expression in the PPL1 neurons. To this end,
170 we visualized $GFP_{11}$-tagged receptors by expressing $GFP_{1-10}$ using *TH-GAL4* (Friggi-Grelin et al.,
171 2003). We detected Dop2R proteins in all MB projections of the PPL1 neurons, whereas Dop1R1
172 proteins were only detectable in the terminals of the PPL1-α3 neuron (Figure 6F and 6G).
173 Strikingly, the starvation-induced changes in the PPL1 neurons were opposite to those in the
174 PAM: Dop2R, but not Dop1R1, significantly increased in the α3 compartment (Figure 6J), and
175 the same tendency was observed in the other PPL1 neurons (Figure6 – figure supplement 1I-L).
176 Taken together, starvation induces opposite responses of dopamine receptor expression in the
177 PPL1 and PAM DANs, and we propose that these changes shift the balance of dopamine output
178 from these subsets (Figure 7A).

179 The starvation-induced increase of Dop2R in the PPL1 terminals suggests enhanced
180 negative feedback (Krashes et al., 2009). If so, loss of Dop2R would impair appetitive memory
181 in starved flies, since inhibition of PPL1 output is necessary for appetitive memory expression

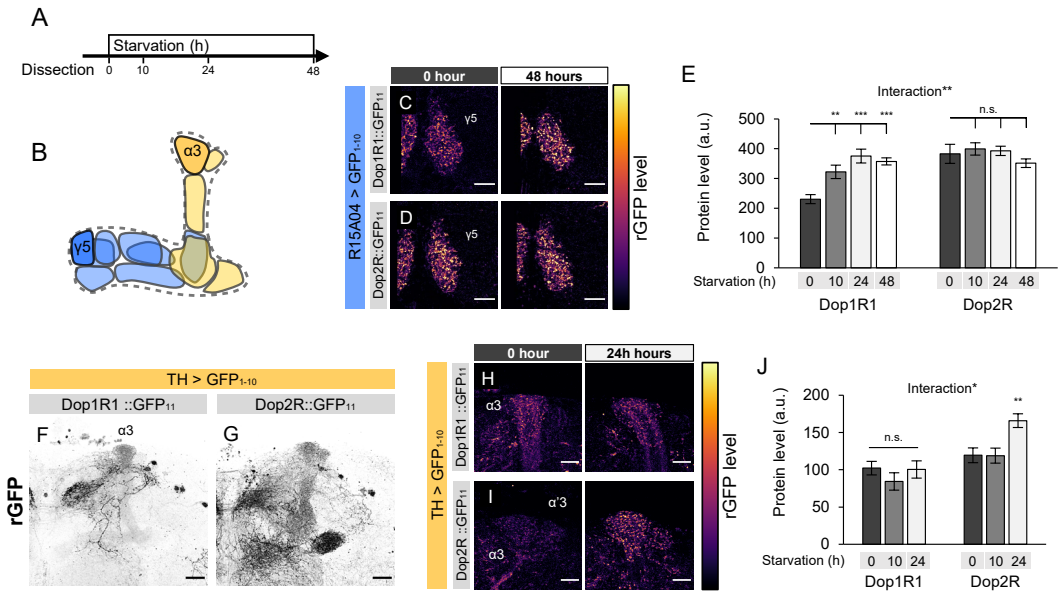


**Figure 6. Bidirectional modification of dopamine receptor expression in dopamine neurons.**

(A) Schematic diagram of the starvation protocol. (B) Schematic illustration of the MB projection of the PAM and PPL1 dopamine neurons marked by *R15A04-GAL4* and *TH-GAL4*.
(C and D) Dop1R (C) and Dop2R (D) in the presynaptic terminals of PAM-γ5 before and after 48 hours of starvation.
(E) Quantification of dopamine receptor levels in the presynaptic terminals of PAM-γ5 after 0, 10, 24 and 48 hours of starvation (n = 6-13).
(F and G) Reconstituted GFP signals of Dop1R1::$GFP_{11}$ (F) and Dop2R::$GFP_{11}$ (G) in the PPL1 neurons. In the MB projections of the PPL1 neurons, Dop1R1 is expressed in only the α3 compartment (F). Dop2R is expressed in all MB projections (G). Maximum-intensity projections of the MB lobe.
(H and I) Dop1R (H) and Dop2R (I) in the presynaptic terminals of PPL1-α3 before and after 24 hours of starvation.
(J) Quantification of the dopamine receptor levels in the presynaptic terminals of PPL1-α3 after 0, 10 and 24 hours of starvation (n = 7-10).
Interaction effects between genotypes and starvation time on protein levels were tested by Two-way ANOVA (E and J).
Scale bar, 10 μm (C, D, H and I), 20 μm (F and G).
Error bars; SEM (E and J). * $p < 0.05$, ** $p < 0.01$, *** $p < 0.001$, n.s. = not significant.

182 (Krashes et al., 2009; Pavlowsky et al., 2018) (Figure 7B). To test this hypothesis, we examined
183 appetitive olfactory associative memory by transgenic knockdown of Dop2R specifically in the
184 PPL1 cluster neurons using *MB504B-GAL4* (Vogt et al., 2014). Indeed, appetitive memory was
185 impaired (Figure 7C), demonstrating the significance of the negative feedback regulation of the
186 PPL1 in appetitive behavior expression. These results are in line with the state-dependent changes
187 in the physiology of these DANs (Siju et al., 2020; Tsao et al., 2018). Taken together, the opposite
188 presynaptic modulation of the PPL1 and PAM neurons through the antagonistic dopamine

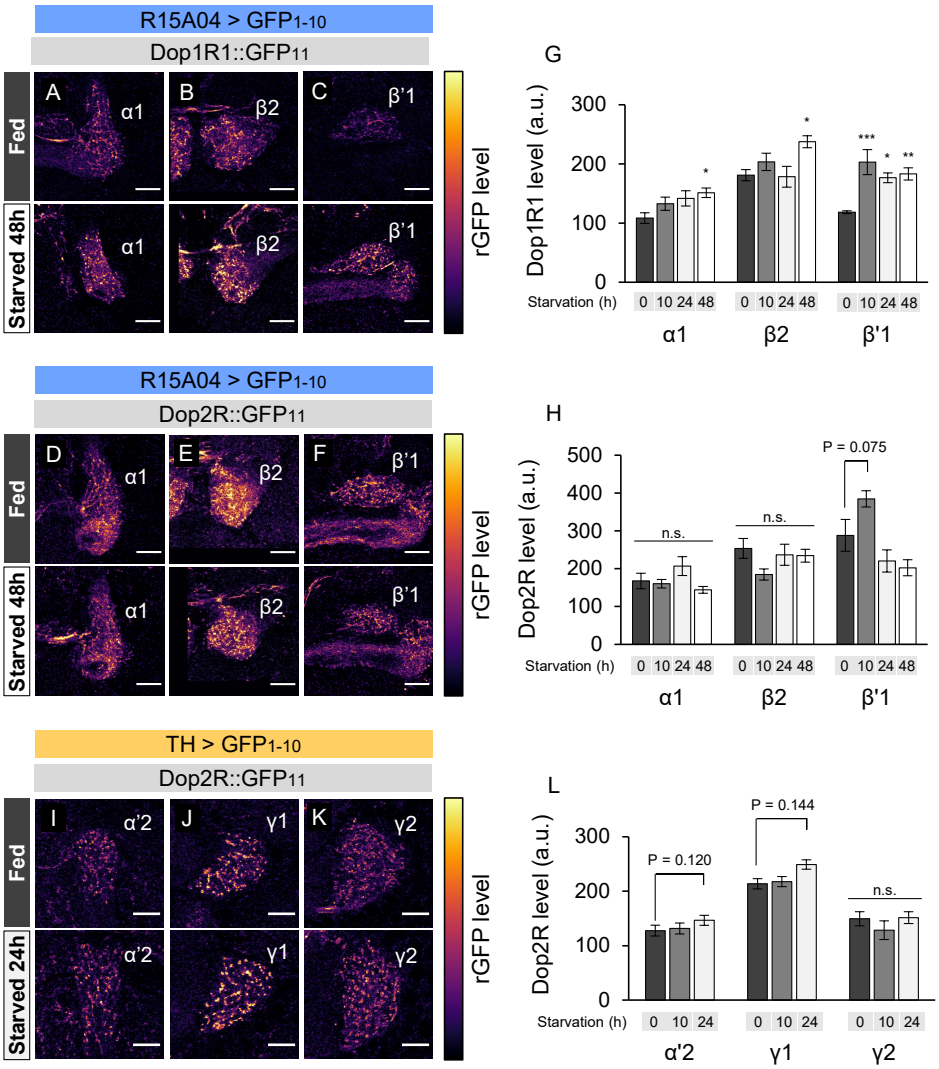


**Figure 6 – figure supplement 1. Starvation-dependent change of dopamine receptors in PAM and PPL1.**

(A-F) Dop1R (A-C) and Dop2R (D-F) in the presynaptic terminals of PAM-α1 (A and D), PAM-β2 (B and E) and PAM-β'1 (C and F) before and after 48 hours of starvation.
(G and H) Quantification of dopamine receptor levels in the presynaptic terminals of the PAM neurons after 0, 10, 24 and 48 hours of starvation (n = 6-13).
(I-K) Dop2R in the presynaptic terminals of PPL1-α'2 (I), PPL1-γ1pedc (J) and PPL1-γ2 (K) before and after 24 hours of starvation.
(L) Quantification of Dop2R levels in the presynaptic terminals of the PPL1 neurons after 0, 10 and 24 hours of starvation (n = 7-10).
Scale bar, 10 µm (A-F, I-K). Error bars; SEM (G, H and L). * $p < 0.05$, ** $p < 0.01$, *** $p < 0.001$, n.s. not significant.

autoreceptors determines the balance of the MB output to control appetitive behaviors.

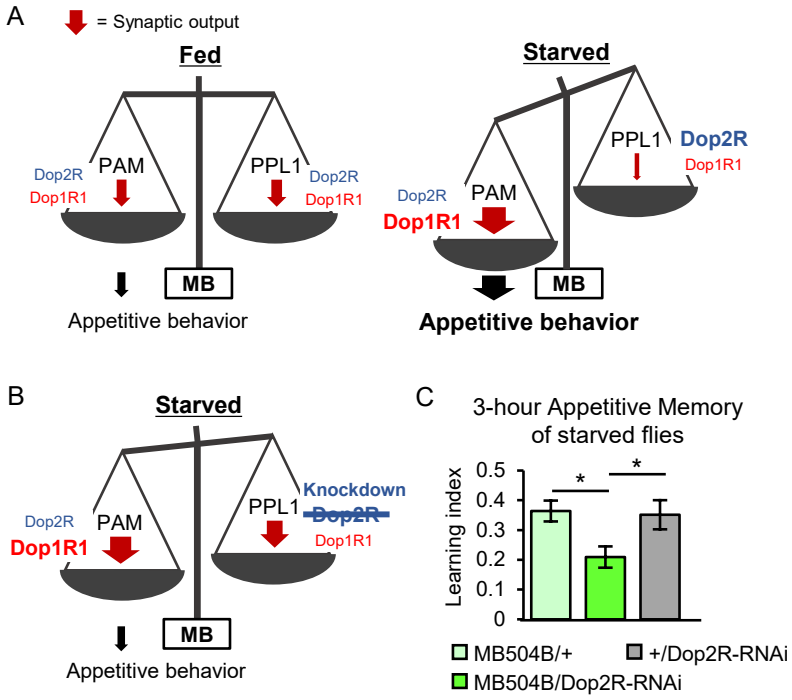


**Figure 7. The dual dopaminergic feedback regulating starved-state dependent expression of appetitive behavior.**

(A) A working model showing the role of the dual dopaminergic feedback regulation. In starved state, increased Dop1R1 in PAM neurons and increased Dop2R in PPL1 neurons changes the balance between the synaptic outputs from these DANs to favor appetitive behavior.
(B) According to the model, loss of Dop2R in PPL1 upregulates output from PPL1 to attenuate appetitive behavior in starved flies.
(C) Knockdown of Dop2R in the PPL1 neurons by *MB504B-GAL4* reduced 3-hour appetitive memory performance (n=14-15). Error bars; SEM. * $p < 0.05$.

190 **Discussion**

191 The present study demonstrated the expression, subcellular localization, and dynamics of
192 endogenous dopamine receptors, specifically Dop1R1 and Dop2R, in the MB circuit of the fly
193 brain. Previously, intronic insertions of fluorescent tags have been used to label endogenous
194 proteins in a cell-type specific manner (Fendl et al., 2020; R. Kamiyama et al., 2021; Williams et
195 al., 2019). CRISPR/Cas9-based insertion is advantageous in terms of flexibility in fusion sites
196 compared to intronic insertions (Fendl et al., 2020; R. Kamiyama et al., 2021; Williams et al.,
197 2019). This enables the C-terminal tagging of dopamine receptors that do not perturb protein
198 localization and function (Kondo et al., 2020).

199 The split-GFP reconstitution strategy enables sensitive detection of low-abundant

200 endogenous proteins by the tandem multimerization of the $GFP_{11}$ tags, as shown in other epitope
201 tags such as SunTag and smFPs (Tanenbaum et al., 2014; Viswanathan et al., 2015). The
202 background fluorescence of the split-GFP fragments was practically negligible. For example,
203 Dop1R1-rGFP signal was observed in fewer cells than $GFP_{1-10}$-expressing PPL1 neurons as
204 expected from the gene expression pattern (D. Kamiyama et al., 2016; Kondo et al., 2020) (Figure
205 6). This approach can thus be applicable to monitor localization and dynamics of endogenous
206 proteins of low abundance.

207 To quantify subcellular receptor localization, we here devised LI, which measures the
208 relative enrichment of tagged proteins over the membrane markers. Quantitative localization
209 analysis with LI revealed fine distinctions in presynaptic enrichment between Dop1R1 and
210 Dop2R (figure 3 and 5). Dop2R showed a stronger association with AZ, while Dop1R1 was
211 distributed more broadly along axons and terminals (Figure 4). Similar but distinct subcellular
212 enrichment of Dop1R1 and Dop2R therefore suggests joint action in intricate regulation of
213 presynaptic dopamine signaling.

214 **Spatial regulation of dopamine signaling through distinct receptor subtypes**

215 How do Dop1R1 and Dop2R function in presynaptic terminals? Differential AZ
216 enrichment suggests differential contributions to the spatial regulation of dopamine response.
217 Dopamine release is not confined to the synaptic cleft, but involves extracellular diffusion (Rice
218 & Cragg, 2008) and extrasynaptic release (Liu & Kaeser, 2019). Such volume transmission can
219 increase the number of target synapses by 10 times (Li et al., 2020; Takemura et al., 2017). The
220 broader distribution of Dop1R1 thus enables to respond to the trace amount of extrasynaptic
221 dopamine. On the other hand, the tight association of Dop2R with the AZ underscores the
222 importance of reducing the noise of second messenger signaling likely through inhibiting
223 activities of adenylyl cyclase and voltage-gated calcium channels (Beaulieu & Gainetdinov, 2011;
224 Hearn et al., 2002). These second messengers, cAMP and $Ca^{2+}$, were reported to regulate distinct
225 aspects of presynaptic functions including release probability and vesicle recycling (Ehmann et
226 al., 2018; Kuromi & Kidokoro, 2000, 2005). The spatial configuration of Dop1R1 and Dop2R
227 may thus contribute to the sensitivity and precision in dopaminergic modulation of the synaptic
228 vesicle cycle.

229 **The dual autoreceptor system may shape dopamine release**

230 Presynaptic localization of Dop1R1 and Dop2R in DANs strongly suggests their functions as
231 autoreceptors. Reported functions of inhibitory dopamine autoreceptors range from negative

232 regulations of the amplitude and kinetics of dopamine transmission, decreasing dopamine
233 synthesis, to altering the uptake of released dopamine (Ford, 2014; Shin & Venton, 2022; Vickrey
234 & Venton, 2011). Considering tight presynaptic Dop2R enrichment in the PAM and PPL1 DANs,
235 such negative feedback should prevent overactivation of second messenger signaling at the AZ,
236 where the ligand concentrations should be highest. In contrast, the presence of Dop1R1 in DAN
237 terminals was unexpected, adding another layer of presynaptic regulations in dopamine release.
238 Although it must be functionally verified if presynaptic Dop1R1 acts as autoreceptors in the PAM
239 and PPL1 DANs, it should provide feedback for the dopamine release. This positive feedback
240 would be particularly necessary in the regions where extracellular dopamine concentrations are
241 low. Indeed, presynaptic Dop1R1 was undetectable in the PPL1 DNAs, which were reported to
242 have high spontaneous activities (Feng et al., 2021; Plaçais & Preat, 2013). Furthermore, we
243 noticed that compositions of presynaptic Dop1R1 and Dop2R vary among individual DANs
244 (Figure 5 and 6). This dual autoreceptor system may thus fine-tune the amplitude and kinetics of
245 dopamine release depending on the cellular function.
246 Dopamine receptor expression is reported to be associated with prolonged exposure to
247 psychoactive substances, such as caffeine and ethanol (Andretic et al., 2008; Kanno et al., 2021;
248 Kondo et al., 2020; Petruccelli et al., 2018). This study further showed starvation-dependent
249 changes of Dop1R1 and Dop2R in DAN terminals (Figure 7). Strikingly, starvation responses of
250 presynaptic Dop1R1 and Dop2R were differential depending on the DAN cell types (Figure 7).
251 We therefore propose the state-dependent bidirectional modulation of the MB output through the
252 dual dopamine autoreceptor system in the PAM and PPL1 neurons (Figure 7A). Starvation
253 changes the dual autoreceptor system to put more weight on the PAM output over PPL1 to control
254 the expression of appetitive behavior (Figure 7A). This shifted balance explains the state-
255 dependent changes in the presynaptic activity of these two clusters of DANs and recruited
256 MBONs for appetitive behavior (Aso, Sitaraman, et al., 2014; Ichinose et al., 2021; Landayan et
257 al., 2018; Owald et al., 2015; Siju et al., 2020; Tsao et al., 2018).

258 **Materials and Methods**

259 **Resource tables**

| Strain | Source | Identifier |
|---|---|---|
| **Antibodies** | | |
| Mouse anti-TH | ImmunoStar Inc., Hudson, WI, USA | Cat# 22941 |
| Mouse anti-Brp | Developmental Studies Hybridoma Bank, Univ. Iowa | nc82 |
| Goat anti-mouse AlexaFluor 633 | Invitrogen, Waltham, MA, USA | Cat# A-21052 |
| ***Drosophila* strain** | | |
| *Dop1R1-T2A-GAL4* | Kondo et al., 2020 | N/A |
| *Dop2R-T2A-GAL4* | Kondo et al., 2020 | N/A |
| *Dop1R1-T2A-LexA* | Kondo et al., 2020 | N/A |
| *Dop2R-T2A-LexA* | Kondo et al., 2020 | N/A |
| *Dop1R1::7xGFP11* | Kondo et al., 2020 | N/A |
| *Dop2R::7xGFP11* | Kondo et al., 2020 | N/A |
| *DopEcR::7xGFP11* | Kondo et al., 2020 | N/A |
| *Dop1R1::Venus* | Kondo et al., 2020 | N/A |
| *Dop2R::Venus* | Kondo et al., 2020 | N/A |
| *UAS-GFP1-10* | Kondo et al., 2020 | N/A |
| *UAS-mCD8::GFP* | Pfeiffer et al., 2012 | BDSC #32194 |
| *lexAop-rCD2::GFP* | Miyamoto et al., 2012 | N/A |
| *UAS-CD4::tdTomato* | C. Han et al., 2011 | BDSC #35841 |
| *UAS-nSyb-CLIP* | Kohl et al., 2014 | BDSC #58398 |
| *Brp::SNAP* | Kohl et al., 2014 | BDSC #58397 |
| *MB-GeneSwitch* | Mao et al., 2004 | BDSC #81013 |
| *R15A04-GAL4* | Pfeiffer et al., 2008 | BDSC #48671 |
| *R58E02-GAL4* | Pfeiffer et al., 2008 | BDSC #41347 |
| *MB504B* | Pfeiffer et al., 2010 | BDSC #68329 |
| *OK371-GAL4* | Mahr & Aberle, 2006 | BDSC #26160 |
| *UAS-Dop2R-RNAi* | Perkins et al., 2015 | BDSC #50621 |
| **Software** | | |
| Fiji | Schindelin et al., 2012, http://fiji.sc | RRID: SCR_002285 |

| | | |
|---|---|---|
| GraphPad Prism 5 | GraphPad Software | RRID: SCR_002798 |

260

261 **Flies**

262 Flies were raised on standard cornmeal food at 25°C under a 12:12 h light-dark cycle (ZT0 at 8
263 AM) for all experiments. The GAL4-UAS system was used to express the transgenes of interest
264 in specific neuron subtypes. Flies carrying GAL4 were crossed to another strain carrying UAS
265 reporters, and F1 progenies were used in the experiments. To visualize $GFP_{11}$-tagged dopamine
266 receptors in the specific cell-types, female fly strains carrying *UAS-CD4::tdTomato*, *UAS-GFP*$_{1-}$
267 $_{10}$ and GAL4 driver was crossed to male fly strains carrying *Dop1R1::GFP*$_{11}$ or *Dop2R::GFP*$_{11}$
268 and F1 progenies were used. To make the giant neuron culture, embryos from *Brp::SNAP* or the
269 F1 progeny of *OK371-GAL4* (BDSC #26160) crossed with *Brp::SNAP, UAS-mCD8::GFP, UAS-*
270 *nSyb-CLIP* flies were used. For the fly lines used in our manuscript, see the Resource Tables.

271 **Brain dissection and Immunohistochemistry**

272 Male flies with the specific genotype were sorted under $CO_2$ anesthesia and kept in a food vial
273 for recovery at least 24 h prior to the dissection. Fly brains were dissected 3-7 days after eclosion
274 in ice-cold Phosphate-buffered saline (PBS). After dissection, brains were kept in ice-cold PBS
275 with 2% paraformaldehyde (PFA) for up to 30 min. For fixation, brains were incubated in 2 %
276 PFA in PBS for 1 hour at room temperature. Fixed brains were washed in PBS with 0.1% Triton
277 X-100 (PBT) for 10 min 3 times. For rGFP imaging, fixed brains were mounted in SeeDB2 (Ke
278 et al., 2016), and native fluorescence was imaged without signal amplification.
279 For chemical tagging reaction (Figure 5A and 5B), brains were incubated in PBT (0.3 %
280 Triton X-100 in PBS) containing CLIP-Surface 547 substrate (1μM, S9233S; New England
281 Biolabs Inc.) for 15 min at room temperature. Brains were washed in PBT for 10 min 3 times.
282 For immunohistochemistry, fixed brains were blocked in 3 % normal goat serum (NGS)
283 for 30 min at room temperature. Brains were incubated in primary and secondary antibodies
284 diluted in PBT with 1 % NGS over two nights at 4 ℃, respectively. After each step, brains were
285 washed three times in PBT for longer than 20 min at room temperature and mounted in 86%
286 glycerol.
287 Following primary antibodies were used: mouse anti-TH (1:100; 22941; ImmunoStar Inc.,
288 Hudson, WI, USA), mouse anti-Brp (1:40; nc82; Developmental Studies Hybridoma Bank, Univ.
289 Iowa). Secondary antibodies: Alexa Fluor 633 goat anti-mouse (1:400 for anti-TH, 1:200 for
290 nc82; A-21052; Invitrogen, Waltham, MA, USA).

291 **Fluorescent imaging**

292 For image acquisition, whole-mount brains were scanned with the Olympus FV1200 confocal
293 microscope with following objective lens; 20x oil (NA = 0.85, UPLSAPO20XO, Olympus), 30x
294 silicone (NA = 1.05, UPLSAPO30XS, Olympus), 40x oil (NA = 1.3, UPLFLN40XO, Olympus),
295 or 60x oil (NA = 1.42, PLAPON60XO, Olympus). Z-stack images were acquired with following
296 voxel sizes; 0.468 x 0.468 x 0.84 $\mu m^3$ for 20x oil (Figure 1A and 1B), 0.099 x 0.099 x 0.44 $\mu m^3$
297 for 30x silicone (Figure 1D-1H), 0.194 x 0.194 x 0.52 $\mu m^3$ for 40x oil (Figure 3B-3G, 6C-6D, 6F-
298 6I and Figure 6 – figure supplement 1 A-F, I-K), and 0.101 x 0.101 x 0.45 $\mu m^3$ for 60x oil (Figure
299 4A, 4B and Figure 4 – figure supplement 1 A-F).

300 For high resolution imaging in Figure 5I-J, Airyscan imaging was performed on Zeiss
301 LSM800 with 63x oil objective lens (NA = 1.40, Plan-Apochromat). A single focal slice was
302 scanned with a pixel size of 0.0425 x 0.0425 $\mu m^2$.

303 **Image analysis**

304 All image analysis were conducted on Fiji (Schindelin et al., 2012).

305 To visualize the subcellular localization of dopamine receptors in defined neurons, we
306 devised the localization index (LI). Relative receptor density was calculated in each voxel by
307 dividing the receptor (reconstituted GFP) signals by the corresponding membrane signals
308 (CD4::tdTomato). To set ROI, any voxels devoid of membrane signal were censored. The local
309 density was normalized by the mean values in the ROI. For the visual representation, the reference
310 membrane signals were colored according to the normalized LI (Figure 2C, middle). To quantify
311 mean LI in each subcellular region (Figure 3H), ROI was manually set at single focal slice that
312 include the largest area of interested region.

313 Three-dimensional iterative deconvolution with the Richardson-Lucy algorithm was
314 applied to some stack images (Figure 4A-B, Figure 4 – figure supplement 1). To generate the
315 theoretical PSF for deconvolution, the ImageJ plug-in diffraction PSF 3D was used. Deconvolved
316 images were used for following colocalization analysis.

317 To analyze the colocalization of dopamine receptors and Brp (Figure 4C), both channels
318 were binarized with the auto-thresholding on Fiji. The ratio of overlap between rGFP and Brp
319 signals over rGFP signals was calculated. Square ROI (10.1 x 10.1 μm, 100 x 100 pixel) at single
320 focal slice was sampled within the tip of the vertical lobes for colocalization analysis.

321 **Embryonic giant neuron culture**

322 Multinucleated giant neurons from neuroblasts were generated as described previously (Wu et al.,

323 1990). Briefly, the interior of a gastrula from stage 6/7 embryo was extracted with a glass
324 micropipette and dispersed into a drop of culture medium (~ 40 μm) on an uncoated coverslip.
325 The culture medium contained 80% *Drosophila* Schneider's insect medium (S0146-100ML,
326 Merck KGaA, Darmstadt, Germany) and 20% fetal bovine serum (F2442-100ML, Merck KGaA,
327 Darmstadt, Germany), with the addition of 50 μg/ml streptomycin, 50 U/ml penicillin (all from
328 Sigma, St. Louis, MO, USA) and cytochalasin B (CCB; 2 μg/ml; Sigma, St. Louis, MO, USA).
329 CCB was removed by washing with CCB-free medium 1 d after plating. All cultures were grown
330 in a humidified chamber.

331 To label Brp::SNAP, cells were incubated in fluorescent SNAP substrate diluted in the
332 culture medium (1:5000, SNAP-Cell 647-SiR, S9102S, Ipswich, MA, USA) for half an hour at
333 RT. For double labeling with nSyb-CLIP, cells were first incubated in fluorescent CLIP substrate
334 diluted in the culture medium (1:5000, CLIP-Cell™ TMR-Star, S9219S, Ipswich, MA, USA) for
335 half an hour at RT. Subsequently, the same cells were labeled by the SNAP substrate to minimize
336 the crosstalk. After the incubation, cells were washed with the culture medium and subjected to
337 confocal scanning with Leica TCS SP8 microscopy equipped with a 40x oil immersion objective
338 (HC PL APO 40x/1.30 Oil PH3 CS2, Leica). Acquired images were then processed with the
339 LIGHTNING software.

340 **Behavioral assays**

341 The experimental protocols were as described previously (Ichinose and Tanimoto., 2016). For
342 appetitive conditioning, a group of approximately 50 flies in a training tube alternately received
343 3-octanol (3OCT; Merck) and 4-methylcyclohexanol (4MCH; Sigma-Aldrich), for 1 minute in a
344 constant air flow with or without reward with an interval of 1 minute between the two odor
345 presentations. These odorants were diluted to 1.2% and 2% with paraffin wax (Sigma-Aldrich),
346 respectively. Dried 2 M sucrose (Sigma-Aldrich) on a piece of filter paper was used as the reward.
347 Flies were starved in the presence of wet tissue paper for 24 hours before appetitive conditioning.
348 For testing, flies were given a choice between CS+ and CS-, which distribution in the plexiglass
349 T-maze (Ichinose and Tanimoto, 2016) was video-recorded one frame per second for 2 minutes
350 with the CMOS cameras (GS3-U3-51S5M, FLIR) with infrared LED illumination (Ichinose &
351 Tanimoto, 2016). Flies were forced to stay on the floor by applying Fluon (Insect-a-Slip PTFE30,
352 BioQuip Products) on the side and top of T-maze arms.

353 Learning index was then calculated by counting the number of flies in each arm using
354 ImageJ macro as described previously (Ichinose and Tanimoto, 2016) with the following formula
355 (Tempel et al., 1983):

$$Learning\ index = \frac{\#_{CS-} - \#_{CS+}}{\#_{CS+} + \#_{CS-}}$$

where $\#_{CS+}$ and $\#_{CS-}$ imply the number of flies in the CS+ and the CS- arms, respectively. Learning index was calculated for every second and was averaged for the last 60 s of the 120 s test session. An average of a pair of reciprocally trained groups was used as a single data point.

**Statistics**

For multiple comparison (Figure 6 and Figure 6 – figure supplement 1), statistics were performed by Prism5 (GraphPad). Data were always first tested for normality (Shapiro-Wilk test) and for homoscedasticity (Spearman's test or Bartlett's test). If these assumptions were not violated, parametric tests (one-way ANOVA, followed by Dunnett's post hoc pairwise test) were applied. If data did not suffice the assumptions for parametric tests, nonparametric tests (Kruskal-Wallis, followed by Dunn's post hoc pairwise test) were performed. For comparison of the two groups, Student's t test (Figure 3H) or Mann-Whitney U test (Figure 4C, 5H) was performed on R Statistical Software.

Bars and error bars represent means and SEM, respectively, in all figures. For all figures, significance corresponds to the following symbols: * $p < 0.05$; ** $p < 0.01$; *** $p < 0.001$; n.s. not significant.

## Funding

| Funder | Grant number | Author |
|---|---|---|
| JST SPRING | JPMJSP2114 | Shun Hiramatsu |
| JSPS KAKENHI | 22H04829 | Hiromu Tanimoto |
| JSPS KAKENHI | 20H00519 | Hiromu Tanimoto |
| JSPS KAKENHI | 22H05481 | Hiromu Tanimoto |
| JSPS KAKENHI | 22KK0106 | Hiromu Tanimoto |
| JSPS KAKENHI | 17H01378 | Hiromu Tanimoto |
| JSPS KAKENHI | 20H03246 | Shu Kondo |
| JSPS KAKENHI | 19KK0383 | Nobuhiro Yamagata |
| JSPS KAKENHI | 17H04765 | Nobuhiro Yamagata |
| Takeda Science Foundation | | Nobuhiro Yamagata |


## Author contributions

H.T. and S.H. conceived the project.
H.T. S.H. and N.Y. designed experiments and interpreted results.
S.K. and H.K. designed, generated, and provided transgenic flies.
H.T and C-F. W. supervised experiments.
S.H., K.S. and N.Y. conducted experiments and analyzed data.
H.T., and S.H. drafted the manuscript.
All authors wrote and revised the manuscript.
All authors read and approved the final manuscript.

## References


Andretic, R., Kim, Y. C., Jones, F. S., Han, K. A., & Greenspan, R. J. (2008). Drosophila D1 dopamine receptor mediates caffeine-induced arousal. *Proceedings of the National Academy of Sciences of the United States of America*, *105*(51), 20392–20397. https://doi.org/10.1073/pnas.0806776105

Aso, Y., Hattori, D., Yu, Y., Johnston, R. M., Iyer, N. A., Ngo, T. T. B., Dionne, H., Abbott, L. F., Axel, R., Tanimoto, H., & Rubin, G. M. (2014). The neuronal architecture of the mushroom body provides a logic for associative learning. *ELife*, *3*, e04577. https://doi.org/10.7554/eLife.04577

Aso, Y., Herb, A., Ogueta, M., Siwanowicz, I., Templier, T., Friedrich, A. B., Ito, K., Scholz, H., & Tanimoto, H. (2012). Three Dopamine pathways induce aversive odor memories with different stability. *PLoS Genetics*, *8*(7). https://doi.org/10.1371/journal.pgen.1002768

Aso, Y., Ray, R. P., Long, X., Bushey, D., Cichewicz, K., Ngo, T. T., Sharp, B., Christoforou, C., Hu, A., Lemire, A. L., Tillberg, P., Hirsh, J., Litwin-Kumar, A., & Rubin, G. M. (2019). Erratum: Correction: Nitric oxide acts as a cotransmitter in a subset of dopaminergic neurons to diversify memory dynamics (eLife (2019) 8 PII: e64094). *ELife*, *9*, 1–33. https://doi.org/10.7554/eLife.64094

Aso, Y., & Rubin, G. M. (2016). Dopaminergic neurons write and update memories with cell-type-specific rules. *ELife*, *5*(JULY), 1–15. https://doi.org/10.7554/eLife.16135

Aso, Y., Sitaraman, D., Ichinose, T., Kaun, K. R., Vogt, K., Belliart-Guérin, G., Plaçais, P. Y., Robie, A. A., Yamagata, N., Schnaitmann, C., Rowell, W. J., Johnston, R. M., Ngo, T. T. B., Chen, N., Korff, W., Nitabach, M. N., Heberlein, U., Preat, T., Branson, K. M., … Rubin, G. M. (2014). Mushroom body output neurons encode valence and guide memory-based action selection in Drosophila. *ELife*, *3*(3), e04580. https://doi.org/10.7554/eLife.04580

Aso, Y., Siwanowicz, I., Bräcker, L., Ito, K., Kitamoto, T., & Tanimoto, H. (2010). Specific dopaminergic neurons for the formation of labile aversive memory. *Current Biology*, *20*(16), 1445–1451. https://doi.org/10.1016/j.cub.2010.06.048

Awasaki, T., Lai, S. L., Ito, K., & Lee, T. (2008). Organization and postembryonic development of glial cells in the adult central brain of Drosophila. *Journal of Neuroscience*, *28*(51), 13742–13753. https://doi.org/10.1523/JNEUROSCI.4844-08.2008

Beaulieu, J. M., & Gainetdinov, R. R. (2011). The physiology, signaling, and pharmacology of dopamine receptors. *Pharmacological Reviews*, *63*(1), 182–217. https://doi.org/10.1124/pr.110.002642

Berry, J. A., Phan, A., & Davis, R. L. (2018). Dopamine Neurons Mediate Learning and

419 Forgetting through Bidirectional Modulation of a Memory Trace. *Cell Reports*, *25*(3), 651-
420 662.e5. https://doi.org/10.1016/j.celrep.2018.09.051
421 Boto, T., Stahl, A., Zhang, X., Louis, T., & Tomchik, S. M. (2019). Independent Contributions of
422 Discrete Dopaminergic Circuits to Cellular Plasticity, Memory Strength, and Valence in
423 Drosophila. *Cell Reports*, *27*(7), 2014-2021.e2.
424 https://doi.org/10.1016/j.celrep.2019.04.069
425 Burke, C. J., Huetteroth, W., Owald, D., Perisse, E., Krashes, M. J., Das, G., Gohl, D., Silies, M.,
426 Certel, S., & Waddell, S. (2012). Layered reward signalling through octopamine and
427 dopamine in Drosophila. *Nature*, *492*(7429), 433–437. https://doi.org/10.1038/nature11614
428 Christiansen, F., Zube, C., Andlauer, T. F. M., Wichmann, C., Fouquet, W., Owald, D., Mertel,
429 S., Leiss, F., Tavosanis, G., Luna, A. J. F., Fiala, A., & Sigrist, S. J. (2011). Presynapses in
430 Kenyon cell dendrites in the mushroom body calyx of Drosophila. *Journal of Neuroscience*,
431 *31*(26), 9696–9707. https://doi.org/10.1523/JNEUROSCI.6542-10.2011
432 Claridge-Chang, A., Roorda, R. D., Vrontou, E., Sjulson, L., Li, H., Hirsh, J., & Miesenböck, G.
433 (2009). Writing Memories with Light-Addressable Reinforcement Circuitry. *Cell*, *139*(2),
434 405–415. https://doi.org/10.1016/j.cell.2009.08.034
435 Cohn, R., Morantte, I., & Ruta, V. (2015). Coordinated and Compartmentalized Neuromodulation
436 Shapes Sensory Processing in Drosophila. *Cell*, *163*(7), 1742–1755.
437 https://doi.org/10.1016/j.cell.2015.11.019
438 Croset, V., Treiber, C. D., & Waddell, S. (2018). Cellular diversity in the Drosophila midbrain
439 revealed by single-cell transcriptomics. *ELife*, *7*, 1–31. https://doi.org/10.7554/eLife.34550
440 Davie, K., Janssens, J., Koldere, D., De Waegeneer, M., Pech, U., Kreft, Ł., Aibar, S., Makhzami,
441 S., Christiaens, V., Bravo González-Blas, C., Poovathingal, S., Hulselmans, G., Spanier, K.
442 I., Moerman, T., Vanspauwen, B., Geurs, S., Voet, T., Lammertyn, J., Thienpont, B., …
443 Aerts, S. (2018). A Single-Cell Transcriptome Atlas of the Aging Drosophila Brain. *Cell*,
444 *174*(4), 982-998.e20. https://doi.org/10.1016/j.cell.2018.05.057
445 Deng, B., Li, Q., Liu, X., Cao, Y., Li, B., Qian, Y., Xu, R., Mao, R., Zhou, E., Zhang, W., Huang,
446 J., & Rao, Y. (2019). Chemoconnectomics: Mapping Chemical Transmission in Drosophila.
447 *Neuron*, *101*(5), 876-893.e4. https://doi.org/10.1016/j.neuron.2019.01.045
448 Dolan, M. J., Frechter, S., Bates, A. S., Dan, C., Huoviala, P., Roberts, R. J., Schlegel, P., Dhawan,
449 S., Tabano, R., Dionne, H., Christoforou, C., Close, K., Sutcliffe, B., Giuliani, B., Li, F.,
450 Costa, M., Ihrke, G., Meissner, G. W., Bock, D. D., … Jefferis, G. S. (2019). Neurogenetic
451 dissection of the drosophila lateral horn reveals major outputs, diverse behavioural functions,
452 and interactions with the mushroom body. *ELife*, *8*, 1–45.

https://doi.org/10.7554/eLife.43079

Ehmann, N., Owald, D., & Kittel, R. J. (2018). Drosophila active zones: From molecules to behaviour. *Neuroscience Research*, *127*, 14–24. https://doi.org/10.1016/j.neures.2017.11.015

Felsenberg, J., Jacob, P. F., Walker, T., Barnstedt, O., Edmondson-Stait, A. J., Pleijzier, M. W., Otto, N., Schlegel, P., Sharifi, N., Perisse, E., Smith, C. S., Lauritzen, J. S., Costa, M., Jefferis, G. S. X. E., Bock, D. D., & Waddell, S. (2018). Integration of Parallel Opposing Memories Underlies Memory Extinction. *Cell*, *175*(3), 709-722.e15. https://doi.org/10.1016/j.cell.2018.08.021

Fendl, S., Vieira, R. M., & Borst, A. (2020). Conditional protein tagging methods reveal highly specific subcellular distribution of ion channels in motion-sensing neurons. *ELife*, *9*, 1–48. https://doi.org/10.7554/eLife.62953

Ford, C. P. (2014). The role of D2-autoreceptors in regulating dopamine neuron activity and transmission. *Neuroscience*, *282*, 13–22. https://doi.org/10.1016/j.neuroscience.2014.01.025

Friggi-Grelin, F., Coulom, H., Meller, M., Gomez, D., Hirsh, J., & Birman, S. (2003). Targeted gene expression in Drosophila dopaminergic cells using regulatory sequences from tyrosine hydroxylase. *Journal of Neurobiology*, *54*(4), 618–627. https://doi.org/10.1002/neu.10185

Gerfen, C. R., & Surmeier, D. J. (2011). Modulation of striatal projection systems by dopamine. *Annual Review of Neuroscience*, *34*, 441–466. https://doi.org/10.1146/annurev-neuro-061010-113641

Han, C., Jan, L. Y., & Jan, Y. N. (2011). Enhancer-driven membrane markers for analysis of nonautonomous mechanisms reveal neuron-glia interactions in Drosophila. *Proceedings of the National Academy of Sciences of the United States of America*, *108*(23), 9673–9678. https://doi.org/10.1073/pnas.1106386108

Han, K. A., Millar, N. S., Grotewiel, M. S., & Davis, R. L. (1996). DAMB, a novel dopamine receptor expressed specifically in Drosophila mushroom bodies. *Neuron*, *16*(6), 1127–1135. https://doi.org/10.1016/S0896-6273(00)80139-7

Handler, A., Graham, T. G. W., Cohn, R., Morantte, I., Siliciano, A. F., Zeng, J., Li, Y., & Ruta, V. (2019). Distinct Dopamine Receptor Pathways Underlie the Temporal Sensitivity of Associative Learning. *Cell*, *178*(1), 60-75.e19. https://doi.org/10.1016/j.cell.2019.05.040

Hanesch, U., Fischbach, K. F., & Heisenberg, M. (1989). Neuronal architecture of the central complex in Drosophila melanogaster. *Cell and Tissue Research*, *257*(2), 343–366. https://doi.org/10.1007/BF00261838

Hearn, M. G., Ren, Y., McBride, E. W., Reveillaud, I., Beinborn, M., & Kopin, A. S. (2002). A Drosophila dopamine 2-like receptor: Molecular characterization and identification of multiple alternatively spliced variants. *Proceedings of the National Academy of Sciences of the United States of America*, *99*(22), 14554–14559. https://doi.org/10.1073/pnas.202498299

Honegger, K. S., Campbell, R. A. A., & Turner, G. C. (2011). Cellular-resolution population imaging reveals robust sparse coding in the drosophila mushroom body. *Journal of Neuroscience*, *31*(33), 11772–11785. https://doi.org/10.1523/JNEUROSCI.1099-11.2011

Huetteroth, W., Perisse, E., Lin, S., Klappenbach, M., Burke, C., & Waddell, S. (2015). Sweet taste and nutrient value subdivide rewarding dopaminergic neurons in drosophila. *Current Biology*, *25*(6), 751–758. https://doi.org/10.1016/j.cub.2015.01.036

Ichinose, T., Kanno, M., Wu, H., Yamagata, N., Sun, H., Abe, A., & Tanimoto, H. (2021). Mushroom body output differentiates memory processes and distinct memory-guided behaviors. *Current Biology*, *31*(6), 1294-1302.e4. https://doi.org/10.1016/j.cub.2020.12.032

Ichinose, T., & Tanimoto, H. (2016). Dynamics of memory-guided choice behavior in Drosophila. *Proceedings of the Japan Academy Series B: Physical and Biological Sciences*, *92*(8), 346–357. https://doi.org/10.2183/pjab.92.346

Ichinose, T., Tanimoto, H., & Yamagata, N. (2017). Behavioral modulation by spontaneous activity of dopamine neurons. *Frontiers in Systems Neuroscience*, *11*(December), 1–12. https://doi.org/10.3389/fnsys.2017.00088

Kamiyama, D., Sekine, S., Barsi-Rhyne, B., Hu, J., Chen, B., Gilbert, L. A., Ishikawa, H., Leonetti, M. D., Marshall, W. F., Weissman, J. S., & Huang, B. (2016). Versatile protein tagging in cells with split fluorescent protein. *Nature Communications*, *7*, 1–9. https://doi.org/10.1038/ncomms11046

Kamiyama, R., Banzai, K., Liu, P., Marar, A., Tamura, R., Jiang, F., Fitch, M. A., Xie, J., & Kamiyama, D. (2021). Cell-type-specific, multicolor labeling of endogenous proteins with split fluorescent protein tags in Drosophila. *Proceedings of the National Academy of Sciences of the United States of America*, *118*(23), 1–11. https://doi.org/10.1073/pnas.2024690118

Kanno, M., Hiramatsu, S., Kondo, S., Tanimoto, H., & Ichinose, T. (2021). Voluntary intake of psychoactive substances is regulated by the dopamine receptor Dop1R1 in Drosophila. *Scientific Reports*, *11*(1), 1–10. https://doi.org/10.1038/s41598-021-82813-0

Ke, M. T., Nakai, Y., Fujimoto, S., Takayama, R., Yoshida, S., Kitajima, T. S., Sato, M., & Imai, T. (2016). Super-Resolution Mapping of Neuronal Circuitry With an Index-Optimized

521 Clearing Agent. *Cell Reports*, *14*(11), 2718–2732.
522 https://doi.org/10.1016/j.celrep.2016.02.057
523 Kohl, J., Ng, J., Cachero, S., Ciabatti, E., Dolan, M.-J., Sutcliffe, B., Tozer, A., Ruehle, S.,
524 Krueger, D., Frechter, S., Branco, T., Tripodi, M., & Jefferis, G. S. X. E. (2014). Ultrafast
525 tissue staining with chemical tags. *Proceedings of the National Academy of Sciences*,
526 *111*(36), E3805–E3814. https://doi.org/10.1073/pnas.1411087111
527 Kondo, S., Takahashi, T., Yamagata, N., Imanishi, Y., Katow, H., Hiramatsu, S., Lynn, K., Abe,
528 A., Kumaraswamy, A., & Tanimoto, H. (2020). Neurochemical Organization of the
529 Drosophila Brain Visualized by Endogenously Tagged Neurotransmitter Receptors. *Cell*
530 *Reports*, *30*(1), 284-297.e5. https://doi.org/10.1016/j.celrep.2019.12.018
531 Krashes, M. J., DasGupta, S., Vreede, A., White, B., Armstrong, J. D., & Waddell, S. (2009). A
532 Neural Circuit Mechanism Integrating Motivational State with Memory Expression in
533 Drosophila. *Cell*, *139*(2), 416–427. https://doi.org/10.1016/j.cell.2009.08.035
534 Kuromi, H., & Kidokoro, Y. (2000). Tetanic stimulation recruits vesicles from reserve pool via a
535 cAMP-mediated process in Drosophila synapses. *Neuron*, *27*(1), 133–143.
536 https://doi.org/10.1016/S0896-6273(00)00015-5
537 Kuromi, H., & Kidokoro, Y. (2005). Exocytosis and endocytosis of synaptic vesicles and
538 functional roles of vesicle pools: Lessons from the Drosophila neuromuscular junction.
539 *Neuroscientist*, *11*(2), 138–147. https://doi.org/10.1177/1073858404271679
540 Landayan, D., Feldman, D. S., & Wolf, F. W. (2018). Satiation state-dependent dopaminergic
541 control of foraging in Drosophila. *Scientific Reports*, *8*(1), 1–9.
542 https://doi.org/10.1038/s41598-018-24217-1
543 Li, F., Lindsey, J. W., Marin, E. C., Otto, N., Dreher, M., Dempsey, G., Stark, I., Bates, A. S.,
544 Pleijzier, M. W., Schlegel, P., Nern, A., Takemura, S., Eckstein, N., Yang, T., Francis, A.,
545 Braun, A., Parekh, R., Costa, M., Scheffer, L. K., … Rubin, G. M. (2020). *The connectome*
546 *of the adult Drosophila mushroom body provides insights into function*. 1–86.
547 Lin, S., Owald, D., Chandra, V., Talbot, C., Huetteroth, W., & Waddell, S. (2014). Neural
548 correlates of water reward in thirsty Drosophila. *Nature Neuroscience*, *17*(11), 1536–1542.
549 https://doi.org/10.1038/nn.3827
550 Liu, C., & Kaeser, P. S. (2019). Mechanisms and regulation of dopamine release. *Current Opinion*
551 *in Neurobiology*, *57*, 46–53. https://doi.org/10.1016/j.conb.2019.01.001
552 Liu, C., Plaąais, P. Y., Yamagata, N., Pfeiffer, B. D., Aso, Y., Friedrich, A. B., Siwanowicz, I.,
553 Rubin, G. M., Preat, T., & Tanimoto, H. (2012). A subset of dopamine neurons signals
554 reward for odour memory in Drosophila. *Nature*, *488*(7412), 512–516.

https://doi.org/10.1038/nature11304

Mahr, A., & Aberle, H. (2006). The expression pattern of the Drosophila vesicular glutamate transporter: A marker protein for motoneurons and glutamatergic centers in the brain. *Gene Expression Patterns*, *6*(3), 299–309. https://doi.org/10.1016/j.modgep.2005.07.006

Mao, Z., & Davis, R. L. (2009). Eight different types of dopaminergic neurons innervate the Drosophila mushroom body neuropil: Anatomical and physiological heterogeneity. *Frontiers in Neural Circuits*, *3*(JUL), 1–17. https://doi.org/10.3389/neuro.04.005.2009

Mao, Z., Roman, G., Zong, L., & Davis, R. L. (2004). Pharmacogenetic rescue in time and space of the rutabaga memory impairment by using Gene-Switch. *Proceedings of the National Academy of Sciences of the United States of America*, *101*(1), 198–203. https://doi.org/10.1073/pnas.0306128101

Masek, P., Worden, K., Aso, Y., Rubin, G. M., & Keene, A. C. (2015). A dopamine-modulated neural circuit regulating aversive taste memory in drosophila. *Current Biology*, *25*(11), 1535–1541. https://doi.org/10.1016/j.cub.2015.04.027

Miyamoto, T., Slone, J., Song, X., & Amrein, H. (2012). A fructose receptor functions as a nutrient sensor in the drosophila brain. *Cell*, *151*(5), 1113–1125. https://doi.org/10.1016/j.cell.2012.10.024

Nässel, D. R., & Elekes, K. (1992). Aminergic neurons in the brain of blowflies and Drosophila: dopamine- and tyrosine hydroxylase-immunoreactive neurons and their relationship with putative histaminergic neurons. *Cell & Tissue Research*, *267*(1), 147–167. https://doi.org/10.1007/BF00318701

Owald, D., Felsenberg, J., Talbot, C. B., Das, G., Perisse, E., Huetteroth, W., & Waddell, S. (2015). Activity of defined mushroom body output neurons underlies learned olfactory behavior in Drosophila. *Neuron*, *86*(2), 417–427. https://doi.org/10.1016/j.neuron.2015.03.025

Pavlowsky, A., Schor, J., Plaçais, P. Y., & Preat, T. (2018). A GABAergic Feedback Shapes Dopaminergic Input on the Drosophila Mushroom Body to Promote Appetitive Long-Term Memory. *Current Biology*, *28*(11), 1783-1793.e4. https://doi.org/10.1016/j.cub.2018.04.040

Perkins, L. A., Holderbaum, L., Tao, R., Hu, Y., Sopko, R., McCall, K., Yang-Zhou, D., Flockhart, I., Binari, R., Shim, H. S., Miller, A., Housden, A., Foos, M., Randkelv, S., Kelley, C., Namgyal, P., Villalta, C., Liu, L. P., Jiang, X., … Perrimon, N. (2015). The transgenic RNAi project at Harvard medical school: Resources and validation. *Genetics*, *201*(3), 843–852. https://doi.org/10.1534/genetics.115.180208

589 Petruccelli, E., Feyder, M., Ledru, N., Jaques, Y., Anderson, E., & Kaun, K. R. (2018). Alcohol
590 Activates Scabrous-Notch to Influence Associated Memories. *Neuron*, *100*(5), 1209-
591 1223.e4. https://doi.org/10.1016/j.neuron.2018.10.005
592 Pfeiffer, B. D., Jenett, A., Hammonds, A. S., Ngo, T. T. B., Misra, S., Murphy, C., Scully, A.,
593 Carlson, J. W., Wan, K. H., Laverty, T. R., Mungall, C., Svirskas, R., Kadonaga, J. T., Doe,
594 C. Q., Eisen, M. B., Celniker, S. E., & Rubin, G. M. (2008). Tools for neuroanatomy and
595 neurogenetics in Drosophila. *Proceedings of the National Academy of Sciences of the United*
596 *States of America*, *105*(28), 9715–9720. https://doi.org/10.1073/pnas.0803697105
597 Pfeiffer, B. D., Ngo, T. T. B., Hibbard, K. L., Murphy, C., Jenett, A., Truman, J. W., & Rubin, G.
598 M. (2010). Refinement of tools for targeted gene expression in Drosophila. *Genetics*, *186*(2),
599 735–755. https://doi.org/10.1534/genetics.110.119917
600 Pfeiffer, B. D., Truman, J. W., & Rubin, G. M. (2012). Using translational enhancers to increase
601 transgene expression in Drosophila. *Proceedings of the National Academy of Sciences of the*
602 *United States of America*, *109*(17), 6626–6631. https://doi.org/10.1073/pnas.1204520109
603 Plaçais, P. Y., & Preat, T. (2013). To favor survival under food shortage, the brain disables costly
604 memory. *Science*, *339*(6118), 440–442. https://doi.org/10.1126/science.1226018
605 Rice, M. E., & Cragg, S. J. (2008). Dopamine spillover after quantal release: Rethinking
606 dopamine transmission in the nigrostriatal pathway. *Brain Research Reviews*, *58*(2), 303–
607 313. https://doi.org/10.1016/j.brainresrev.2008.02.004
608 Riemensperger, T., Völler, T., Stock, P., Buchner, E., & Fiala, A. (2005). Punishment prediction
609 by dopaminergic neurons in Drosophila. *Current Biology*, *15*(21), 1953–1960.
610 https://doi.org/10.1016/j.cub.2005.09.042
611 Saito, M., & Wu, C. F. (1991). Expression of ion channels and mutational effects in giant
612 Drosophila neurons differentiated from cell division-arrested embryonic neuroblasts.
613 *Journal of Neuroscience*, *11*(7), 2135–2150. https://doi.org/10.1523/jneurosci.11-07-
614 02135.1991
615 Schindelin, J., Arganda-Carreras, I., Frise, E., Kaynig, V., Longair, M., Pietzsch, T., Preibisch,
616 S., Rueden, C., Saalfeld, S., Schmid, B., Tinevez, J. Y., White, D. J., Hartenstein, V., Eliceiri,
617 K., Tomancak, P., & Cardona, A. (2012). Fiji: An open-source platform for biological-image
618 analysis. *Nature Methods*, *9*(7), 676–682. https://doi.org/10.1038/nmeth.2019
619 Senapati, B., Tsao, C. H., Juan, Y. A., Chiu, T. H., Wu, C. L., Waddell, S., & Lin, S. (2019). A
620 neural mechanism for deprivation state-specific expression of relevant memories in
621 Drosophila. *Nature Neuroscience*, *22*(12), 2029–2039. https://doi.org/10.1038/s41593-019-
622 0515-z

Shin, M., & Venton, B. J. (2022). Fast-Scan Cyclic Voltammetry (FSCV) Reveals Behaviorally Evoked Dopamine Release by Sugar Feeding in the Adult Drosophila Mushroom Body. *Angewandte Chemie - International Edition*, *61*(44), 1–5. https://doi.org/10.1002/anie.202207399

Siju, K. P., Štih, V., Aimon, S., Gjorgjieva, J., Portugues, R., & Grunwald Kadow, I. C. (2020). Valence and State-Dependent Population Coding in Dopaminergic Neurons in the Fly Mushroom Body. *Current Biology*, *30*(11), 2104-2115.e4. https://doi.org/10.1016/j.cub.2020.04.037

Srivastava, D. P., Yu, E. J., Kennedy, K., Chatwin, H., Reale, V., Hamon, M., Smith, T., & Evans, P. D. (2005). Rapid, nongenomic responses to ecdysteroids and catecholamines mediated by a novel Drosophila G-protein-coupled receptor. *Journal of Neuroscience*, *25*(26), 6145–6155. https://doi.org/10.1523/JNEUROSCI.1005-05.2005

Sugamori, K. S., Demchyshyn, L. L., McConkey, F., Forte, M. A., & Niznik, H. B. (1995). A primordial dopamine D1-like adenylyl cyclase-linked receptor from Drosophila melanogaster displaying poor affinity for benzazepines. *FEBS Letters*, *362*(2), 131–138. https://doi.org/10.1016/0014-5793(95)00224-W

Takemura, S. ya, Aso, Y., Hige, T., Wong, A., Lu, Z., Xu, C. S., Rivlin, P. K., Hess, H., Zhao, T., Parag, T., Berg, S., Huang, G., Katz, W., Olbris, D. J., Plaza, S., Umayam, L., Aniceto, R., Chang, L. A., Lauchie, S., … Scheffer, L. K. (2017). A connectome of a learning and memory center in the adult Drosophila brain. *ELife*, *6*, 1–43. https://doi.org/10.7554/eLife.26975

Tanaka, N. K., Tanimoto, H., & Ito, K. (2008). Neuronal assemblies of the Drosophila mushroom body. *Journal of Comparative Neurology*, *508*(5), 711–755. https://doi.org/10.1002/cne.21692

Tanenbaum, M. E., Gilbert, L. A., Qi, L. S., Weissman, J. S., & Vale, R. D. (2014). A protein-tagging system for signal amplification in gene expression and fluorescence imaging. *Cell*, *159*(3), 635–646. https://doi.org/10.1016/j.cell.2014.09.039

Tempel, B. L., Bonini, N., Dawson, D. R., & Quinn, W. G. (1983). Reward learning in normal and mutant Drosophila. *Proceedings of the National Academy of Sciences of the United States of America*, *80*(5 I), 1482–1486. https://doi.org/10.1073/pnas.80.5.1482

Tsao, C. H., Chen, C. C., Lin, C. H., Yang, H. Y., & Lin, S. (2018). Drosophila mushroom bodies integrate hunger and satiety signals to control innate food-seeking behavior. *ELife*, *7*, 1–35. https://doi.org/10.7554/eLife.35264

Turner, G. C., Bazhenov, M., & Laurent, G. (2008). Olfactory representations by Drosophila

mushroom body neurons. *Journal of Neurophysiology*, *99*(2), 734–746. https://doi.org/10.1152/jn.01283.2007

Vickrey, T. L., & Venton, B. J. (2011). Drosophila dopamine2-like receptors function as autoreceptors. *ACS Chemical Neuroscience*, *2*(12), 723–729. https://doi.org/10.1021/cn200057k

Viswanathan, S., Williams, M. E., Bloss, E. B., Stasevich, T. J., Speer, C. M., Nern, A., Pfeiffer, B. D., Hooks, B. M., Li, W. P., English, B. P., Tian, T., Henry, G. L., Macklin, J. J., Patel, R., Gerfen, C. R., Zhuang, X., Wang, Y., Rubin, G. M., & Looger, L. L. (2015). High-performance probes for light and electron microscopy. *Nature Methods*, *12*(6), 568–576. https://doi.org/10.1038/nmeth.3365

Vogt, K., Schnaitmann, C., Dylla, K. V., Knapek, S., Aso, Y., Rubin, G. M., & Tanimoto, H. (2014). Shared mushroom body circuits underlie visual and olfactory memories in Drosophila. *ELife*, *3*, e02395. https://doi.org/10.7554/eLife.02395

Wagh, D. A., Rasse, T. M., Asan, E., Hofbauer, A., Schwenkert, I., Dürrbeck, H., Buchner, S., Dabauvalle, M. C., Schmidt, M., Qin, G., Wichmann, C., Kittel, R., Sigrist, S. J., & Buchner, E. (2006). Bruchpilot, a protein with homology to ELKS/CAST, is required for structural integrity and function of synaptic active zones in Drosophila. *Neuron*, *49*(6), 833–844. https://doi.org/10.1016/j.neuron.2006.02.008

Williams, J. L., Shearin, H. K., & Stowers, R. S. (2019). Conditional synaptic vesicle markers for drosophila. *G3: Genes, Genomes, Genetics*, *9*(3), 737–748. https://doi.org/10.1534/g3.118.200975

Wu, C. -F, Sakai, K., Saito, M., & Hotta, Y. (1990). Giant Drosophila neurons differentiated from cytokinesis-arrested embryonic neuroblasts. *Journal of Neurobiology*, *21*(3), 499–507. https://doi.org/10.1002/neu.480210310

Yamagata, N., Hiroi, M., Kondo, S., Abe, A., & Tanimoto, H. (2016). Suppression of Dopamine Neurons Mediates Reward. *PLoS Biology*, *14*(12), 1–16. https://doi.org/10.1371/journal.pbio.1002586

Yamagata, N., Ichinose, T., Aso, Y., Plaçais, P.-Y., Friedrich, A. B., Sima, R. J., Preat, T., Rubin, G. M., & Tanimoto, H. (2015). Distinct dopamine neurons mediate reward signals for short- and long-term memories. *Proceedings of the National Academy of Sciences*, *112*(2), 578–583. https://doi.org/10.1073/pnas.1421930112

Yao, W. D., Rusch, J., Poo, M. M., & Wu, C. F. (2000). Spontaneous acetylcholine secretion from developing growth cones of Drosophila central neurons in culture: Effects of cAMP-pathway mutations. *Journal of Neuroscience*, *20*(7), 2626–2637.

https://doi.org/10.1523/jneurosci.20-07-02626.2000